Salvatore *et al. Nanoscale Research Letters* (2017) 12:167
DOI 10.1186/s11671-017-1930-2

Nanoscale Research Letters

NANO EXPRESS Open Access

Synthesis and Characterization of Highly Intercalated Graphite Bisulfate

Marcella Salvatore[1,2], Gianfranco Carotenuto[1], Sergio De Nicola[3*], Carlo Camerlingo[3], Veronica Ambrogi[1,2] and Cosimo Carfagna[1,2]

Abstract

Different chemical formulations for the synthesis of highly intercalated graphite bisulfate have been tested. In particular, nitric acid, potassium nitrate, potassium dichromate, potassium permanganate, sodium periodate, sodium chlorate, and hydrogen peroxide have been used in this synthesis scheme as the auxiliary reagent (oxidizing agent). In order to evaluate the presence of delamination, and pre-expansion phenomena, and the achieved intercalation degree in the prepared samples, the obtained graphite intercalation compounds have been characterized by scanning electron microscopy (SEM), energy-dispersive X-ray spectroscopy (EDS), X-ray powder diffraction (XRD), infrared spectroscopy (FT-IR), micro-Raman spectroscopy (μ-RS), and thermal analysis (TGA). Delamination and pre-expansion phenomena were observed only for nitric acid, sodium chlorate, and hydrogen peroxide, while the presence of strong oxidizers ($KMnO_4$, $K_2Cr_2O_7$) led to stable graphite intercalation compounds. The largest content of intercalated bisulfate is achieved in the intercalated compounds obtained from $NaIO_4$ and $NaClO_3$.

Keywords: Graphite intercalation compounds, Graphite bisulfate, Nano graphite, Micro-Raman spectroscopy, Fourier transform IR spectroscopy

Background

Graphite intercalation compounds (GICs) are technologically useful functional materials made of graphite flakes uniformly embedding small molecules or metal ions between the graphene sheets [1–5]. Such materials have been intensively studied because of the "staging phenomenon" [6] and the manifold anomalous physicochemical behaviors [3–12]. In addition, GICs are very important in graphite manufacturing [13] and potentially useful in other industrial fields like that of superconductors [14, 15], heterogeneous catalysts [16], anode materials [17], and pyrophoric reactants stabilization [17]. Currently, GICs are used in the preparation of expandable graphite, graphite nanoplatelets (GNP), and single-layer graphene [18–21]. Graphite nitrate and graphite bisulfate have the ability to significantly expand by thermal heating. Owing to the intercalation/expansion processes, the π-π interactions, acting along the graphite c-crystallographic direction, are significantly weakened. Therefore, graphite fragmentations in separated nanocrystals take place by simply applying some sono-acustic energy. The resulting graphite nanocrystal thickness is depending on the GICs intercalation degree, usually classified in terms of "staging" index m, i.e., the number of graphite layers between two intercalant layers [2]; and consequently, the highest "staging index" is required in the graphene preparation. Depending on nature of the intercalating agent, the type of oxidant, and the experimental conditions, it is possible to obtain GICs as "stage I", "stage II", and "stage III" [14]. In particular, in a stage I compound, a single layer of graphene is alternated regularly with intercalated species. In a second stage (third stage, etc.), compound with two (three, etc.) graphene layers are separated by layers of intercalation [22]. According to the literature [23, 24], expandable graphite can be prepared by using various types of GICs hosting Brønsted acids (e.g., sulfuric acid, nitric acid, and acetic acid), metal chlorides ($FeCl_3$, $CuCl_3$, and $ZnCl_2$) [25], gold [26], metals (Na), and alkali metals (Li, Cs, and K) in tetrahydrofuran (THF) [27, 28]. Firstly, C. Schafhäutl [29] and B. Brodie in 1851 [30] described the graphite

*Correspondence: sergio.denicola@spin.cnr.it
[3]CNR-SPIN, Institute for Superconductors, Innovative Materials and Devices, S.S. Napoli, Complesso Universitario di M.S. Angelo, Via Cinthia, 80126 Naples, Italy
Full list of author information is available at the end of the article

bisulfate synthesis based on the following reaction scheme [23]:

$$24nC + O_x{}^z + mH_2SO_4 \rightarrow C_{24}{}^+ \cdot HSO_4{}^- \times (m-1)H_2SO_4 + HO_x{}^{(z-1)} \quad (1)$$

where O_x is the oxidizing agent and C is the carbon atoms in the graphite. Therefore, graphite bisulfate compounds consist of graphite layers intercalated by HSO_4^- and H_2SO_4 molecules [23]. The stage and kinetics of bisulfate formation depend on the sulfuric acid concentration and on the type of oxidizing agent involved in the reactive system [23, 31]. At that time, very limited structural information were given in the literature concerning these systems, since X-ray diffraction was one of the few available characterization approaches. Here, graphite bisulfate has been prepared by classical liquid-phase synthesis techniques and some new reaction scheme based on never investigated oxidizing agents. The achieved materials have been fully characterized regarding their morphology and structure by scanning electron microscopy (SEM), energy-dispersive X-ray spectroscopy (EDS), X-ray powder diffraction (XRD), infrared spectroscopy (FT-IR), micro-Raman spectroscopy (μ-RS), and thermogravimetric analysis (TGA).

Methods

The different graphite bisulfates were synthesized by treating graphite flakes with an oxidizing agent/sulfuric acid mixture (see Table 1). In particular, a glass flask placed in a thermostatic bath was used as reactor. Slow air-bubbling was applied to homogenize the system during the reaction. The reaction time was 1 h, and a 9:1 by volume H_2SO_4/oxidizing agent ratio was selected for all compositions. Such a small amount of oxidizing agent is enough to induce intercalation. The reactions were performed in isothermal condition at the temperatures indicated in Table 1. Constant quantities of graphite flakes (2 g, Aldrich, > 100 mesh), sulfuric acid (40 ml), and oxidizing agent molar amounts were used. Cold deionized water was added to reactive mixture to end the reaction. The selected temperatures were different since oxidizers have a different reactivity.

FT-IR and micro-Raman (μ-RS) spectroscopies were used to analyze the chemical structure of pure graphite and "as prepared" graphite bisulfates. FT-IR were recorded with a PerkinElmer Frontier FT-IR spectrometer, in the range 4000–800 cm^{-1} with 4 cm^{-1} resolution and 6 scans. The KBr pressed disc technique (1 mg of sample and 160 mg of KBr) was used. The KBr was first heated in a furnace overnight at 120 °C to minimize the amount of the adsorbed water. A Jobin-Yvon system from Horiba ISA, with a Triax 180 monochromator, equipped with a liquid nitrogen cooled charge-coupled detector was used for the μ-RS measurements. The grating of 1800 grooves/mm allows a final spectral resolution of 4 cm^{-1}. The spectra were recorded in air at room temperature using a 17 mW He-Ne laser source (wavelength 632.8 nm). The spectrum accumulation time was 120 s. The laser light was focused to a 2 μm spot size on the sample through an Olympus microscope with $\times$100 optical objective. The spectra obtained were analyzed in terms of convoluted Lorentzian functions by using a best-fitting routine of GRAMS/AI (2001, Thermo Electron) program, which is based on the Levenberg-Marquardt nonlinear least-square methods. Wide-angle X-ray powder diffraction (XRD) measurements were performed using a Philips XPW diffractometer with Cu Kα radiation (1.542 Å) filtered by nickel. The scanning rate was 0.02°/s, and the scanning angle was from 5 to 45°. A SEM (Philips model XL20) was used to investigate the morphology. EDS analysis (model Inca Oxford 250) was carried out to confirm the presence of the intercalating agent between graphite layers. The thermal expansion threshold of the different intercalation compounds was measured by thermogravimetric analysis (TGA), using a TA Q5000 instrument equipped with an infrared furnace. TGA measurements were performed using about 1.0/1.8 mg of the sample inserted in an alumina crucible placed in a platinum pan. We adopted such method in order to prevent the leakage of the sample during the expansion phenomenon. The experiments were performed under fluxing nitrogen (flow rate of 25 mL/min).

Table 1 Oxidizing agent used in the reactive mixtures with H_2SO_4 and experimental conditions

Agent	HNO_3	KNO_3	H_2O_2	$KMnO_4$
Temperature reaction (°C)	40	30	40	30
Agent	$K_2Cr_2O_7$	$NaIO_4$	$NaClO_3$	
Temperature reaction (°C)	30	40	30	

Results and Discussion

The morphology of graphite flakes after the oxidation/intercalation treatment has been investigated by comparing SEM micrographs of different GICs to that of starting graphite flakes. The obtained images are reported in Fig. 1. Treatments with H_2SO_4/oxidant lead to intercalated graphite. In addition to the erosion phenomenon also a delamination and pre-expansion were clearly visible for some samples. The image of a natural graphite single flake, reported in Fig. 1a, shows that the flake layers are really close to each other, and the surface is flat and uniform. Figures 1b, f show the GICs obtained using HNO_3 and $K_2Cr_2O_7$ as oxidizer agent. From these images, in addition to intercalation, it is possible to observe a "delamination" phenomenon that is probably due to the strong oxidation effect. When KNO_3 is used as an oxidizer

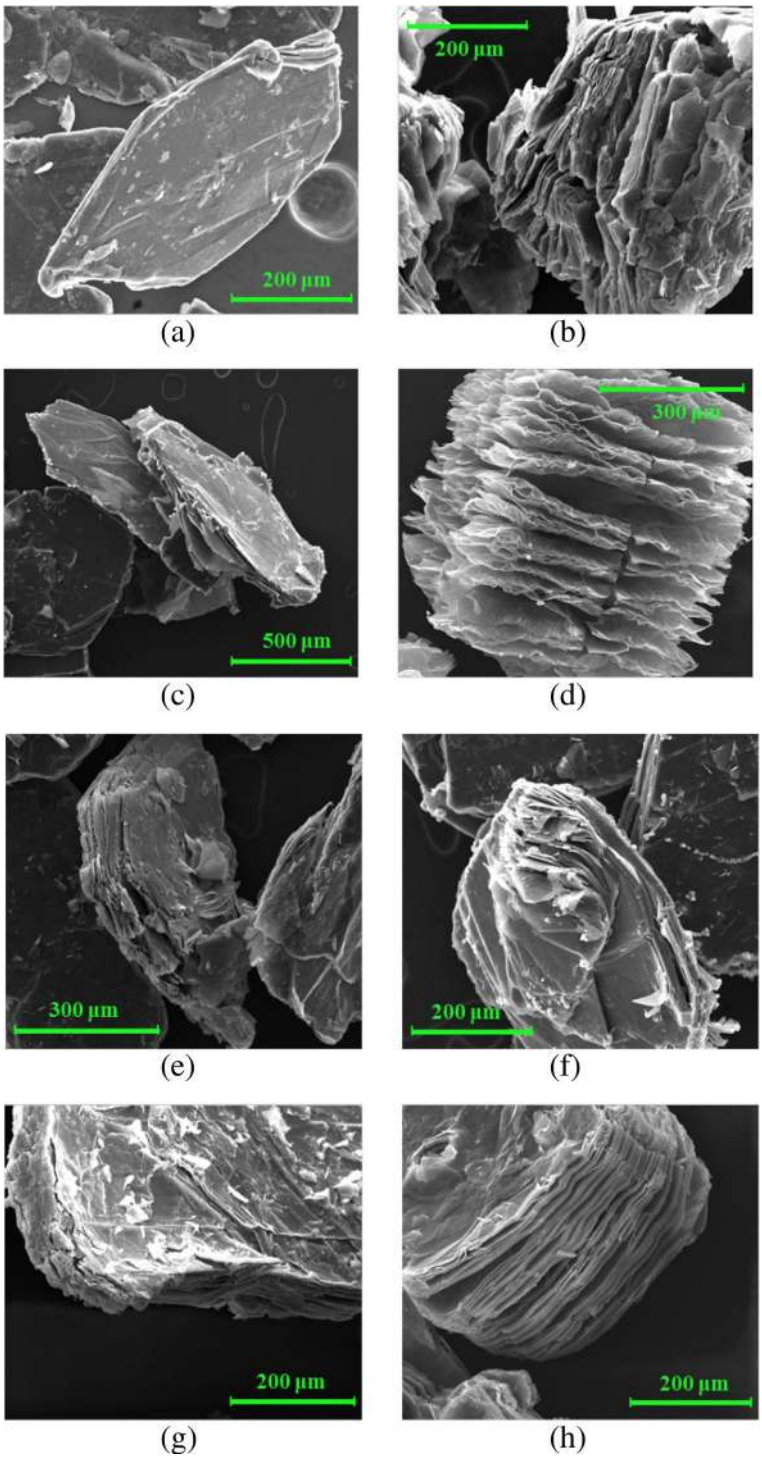

Fig. 1 Scanning electron micrographs (SEM) of **a** starting graphite flakes, GIC from **b** HNO_3, **c** KNO_3, **d** H_2O_2, **e** $KMnO_4$, **f** $K_2Cr_2O_7$, **g** $NaIO_4$, and **h** $NaClO_3$

(Fig. 1c), only a light intercalation phenomenon occur. In this case, small white particles are observed on the intercalated flakes, probably resulting from the KNO_3 crystals not dissolved during the chemical treatment. Furthermore, Fig. 1d shows an image of the GIC resulting from the reaction with H_2O_2 as oxidizing agent. In this case, a graphite pre-expansion phenomenon occurred during the intercalation process. Such a phenomenon is

probably related to the H_2O_2 decomposition to H_2O and O_2 which takes place at room temperature. Figure 1e, g show the images of GICs obtained from $KMnO_4$ and $NaIO_4$, respectively. In this case, it is possible to observe the erosion of the flake boundary. This morphology is tightly connected with the intercalation process although a layer separation is not evident as in the cases of the other samples. The GIC obtained using $NaClO_3$ as an oxidizing agent, Fig. 1h, shows a strong intercalation phenomenon. From this image, it is possible to recognize multiple layers forming the flake. EDS microanalysis was carried out on small sample areas to determine nature and percentage of the elements present in the flake. As an example, we report the data of EDS spectrum from graphite and GIC obtained by HNO_3. In Fig. 2a, b are indicated the positions where EDS analysis has been performed on the graphite and on the GIC (HNO_3) surface, respectively. The elemental composition for each EDS spectrum is reported in Table 2. In natural graphite, it can be clearly seen only the presence of the element carbon (besides some impurities). The EDS spectra of the other GIC samples detected a significant quantity of sulfur and oxygen due to the oxidation/intercalation process.

The structural characteristics of the obtained GICs can be evaluated by comparing XRD diffractograms of pure graphite and GICs. In Fig. 3a, we report the diffractogram of pure graphite, and in Fig. 3b, a portion of the same diffractogram compared with those of the GICs. As visible, the signal of GICs is significantly different from that of natural graphite. The (002) signal, which is the only one visible in the XRD pattern of natural graphite, represents reflections in the perpendicular direction (*c*-axis) of the graphite hexagonal planes. The (002) peak in the GICs X-ray diffractograms is clearly broadened compared to that of the pure graphite. Furthermore, the (002) peak results shifted to lower angles for all studied GICs compared to the pure graphite case. This result is probably due to the presence of defects in the GICs crystal lattice. This effect depends on the obtained intercalation and on the kind of oxidizing agents used in the reaction. In particular, the X-ray diffractograms of GICs obtained using $NaClO_3$, KNO_3, and $K_2Cr_2O_7$ as oxidizing agents show the maximum 2θ shift of the (002) peak. The XRD spectra of GICs by HNO_3 and H_2O_2 exhibit maximum broadening of the (002) peak. As it can be seen from the corresponding SEM images (Fig. 1b, d), the samples appear to be better expanded compared to the other GICs. We ascribe the better expansion to the instability of the HNO_3 and H_2O_2 oxidants which results in gas formation during the intercalation reactions. The oxidation of GIC samples was investigated by FT-IR spectroscopy. Fig. 4 shows FT-IR spectra of prepared samples; as visible, the GIC spectra are remarkably different from that of natural graphite. They exhibit an oxidation signal due to

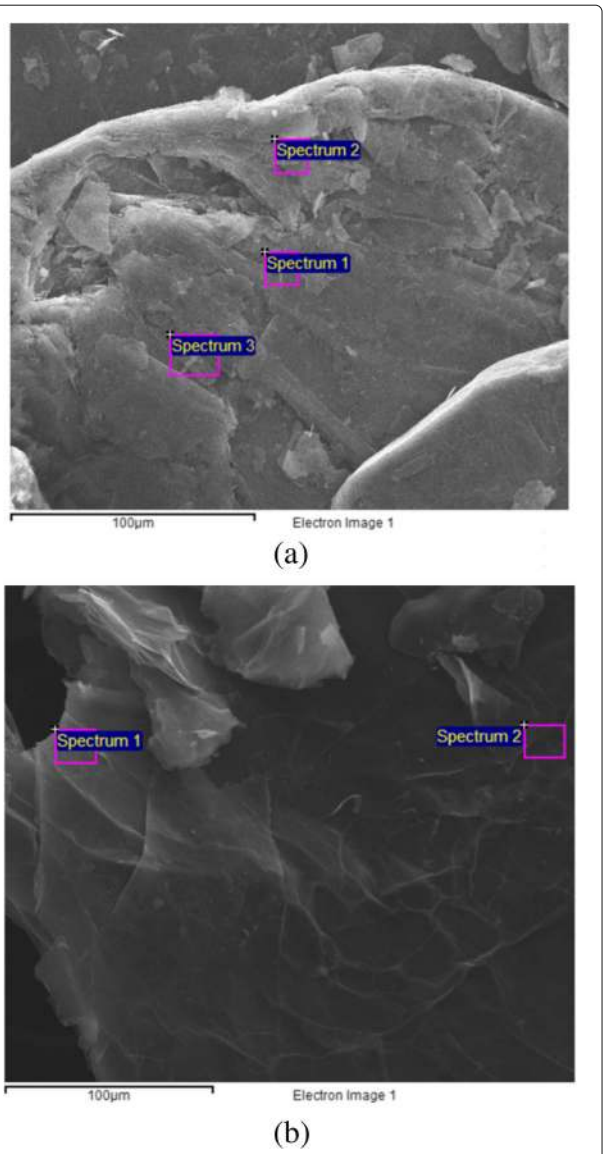

Fig. 2 Positions where EDS analysis has been performed on **a** starting graphite flakes and **b** GIC from HNO_3. The elemental composition is reported in Table 2

Table 2 EDS analysis: elemental composition. Results in weight %

	Spectrum	C	O	S	Si	Other	Total
	Spectrum 1	100.00	–	–	–	–	100.00
Graphite	Spectrum 2	99.50	–	–	0.50	–	100.00
(Fig. 2a)	Spectrum 3	99.56	–	–	0.44	–	100.00
GIC (HNO_3)	Spectrum 1	75.48	21.83	2.32	0.07	0.30	100.00
(Fig. 2b)	Spectrum 2	70.37	21.46	7.93	0.07	0.24	100.00

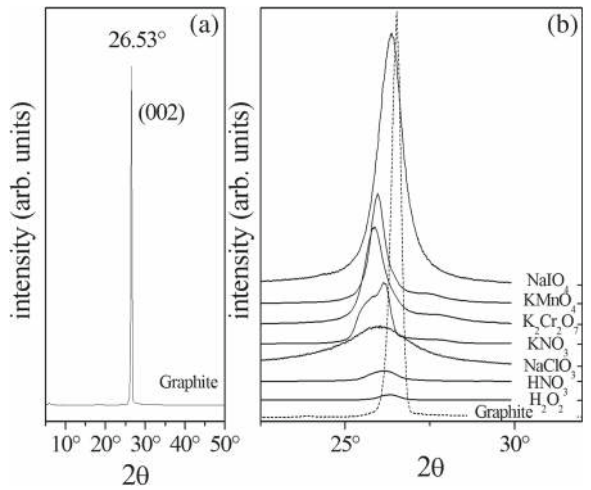

Fig. 3 XRD of graphite and GICs. XRD (002) peak of pure graphite (**a**) and GICs (**b**).The curves in **b** are shifted arbitrarily along the *y*-axis

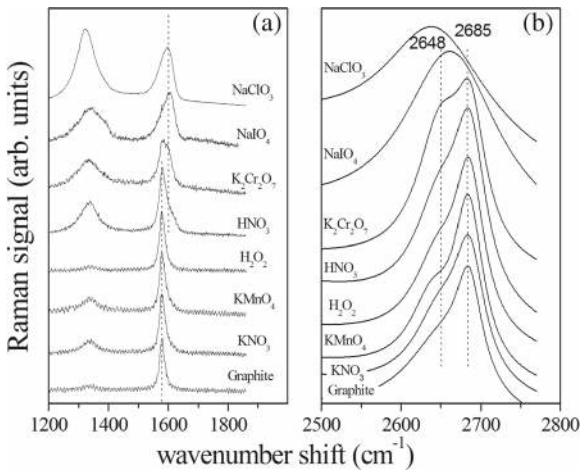

Fig. 5 μ-RS of GICs in the spectral range of 1200–1850 cm^{-1} (**a**) and 2500–2800 cm^{-1} (**b**) . The spectra are shifted arbitrarily along the *y*-axis. The *dotted lines* indicate the spectral position of the main components observed for G (**a**) and 2D mode (**b**), respectively

the presence of hydroxyl groups (−OH) at 3500 cm^{-1}. The natural graphite also presents a light oxidation. The oxidation degree was depending on the type of oxidizer used and has a maximum for $NaClO_3$ and a minimum for the KNO_3 oxidizer. All spectra also featured a clear signal at 1650 cm^{-1} ascribed to the C=C double bond stretching vibration and C–O bond stretching vibration at 1200 cm^{-1}. The μ-RS spectra obtained from the graphite intercalated compounds are reported in Fig. 5 and compared with spectrum of pure graphite. In Fig. 5a, the spectrum region in the wavenumber range of 1200–1850 cm^{-1} is considered, where a prominent peak (designated as G mode) is generated by graphite at about 1582 cm^{-1}. This peak is clearly visible in the spectrum of graphite, reported in the low part of the figure, and in all other spectra, even if evident differences occur in the observed Raman response. The spectra in Fig. 5 are sorted in increasing degree of differentiation with respect to that of graphite. The spectra of the samples obtained from KNO_3, $KMnO_4$, and H_2O_2 look rather similar to that of graphite even if the higher intensity of Raman mode visible at about 1332 cm^{-1} (D mode) manifests the occurrence of a relatively large amount of defects in the lattice [32]. For the samples obtained from KNO_3, H_2O_2, and $KMnO_4$, the Raman G mode can be successfully fitted by a single Lorentzian function centered at about 1580 cm^{-1}. This is not the case of the other spectra (related to $K_2Cr_2O_7$, HNO_3, $NaIO_4$, and $NaClO_3$), where the fit require two distinct components, represented by Lorentzian functions centered at about 1580 cm^{-1} and 1600 cm^{-1}, respectively. Two dotted lines indicate these positions in Fig. 5a. The first component has a center value close to the G mode position of pristine graphite and is assigned to block of not intercalated graphite layers, while the 1600 cm^{-1} mode is assigned to graphene layers next to an intercalant layer. The ratio of the intensity of this second component with respect to the intensity of 1580 cm^{-1} mode, evaluated by the fit procedure, gradually increases from the value of 0.32 for sample $K_2Cr_2O_7$ to the value of 1.33 of sample $NaClO_3$, indicating a significant intercalation degree of the samples, even if in different stage configurations.

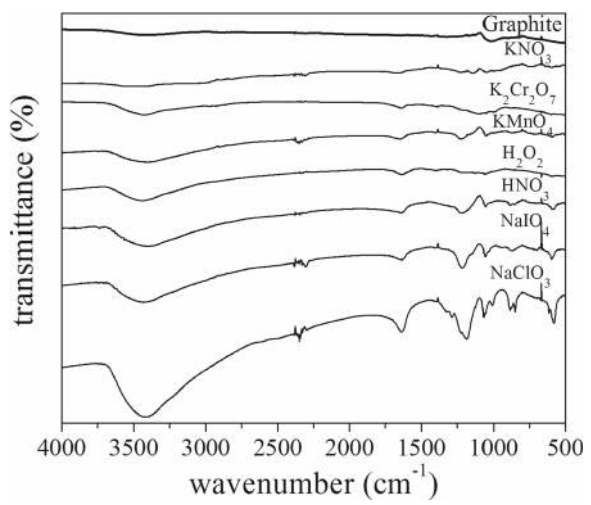

Fig. 4 FT-IR spectroscopy. FT-IR spectra of pure graphite and GICs. The spectra are shifted arbitrarily along the *y*-axis

For these compounds, the intensity of the D mode (at 1332 cm^{-1}) is also clearly observable in the Raman spectra (see Fig. 5a), and it is relatively larger than in the case of GICs before considered (KNO_3, $KMnO_4$, and H_2O_2),

indicating the occurrence of structural defects. This is also evidenced by the slight increase of both the position and the width of the G peak, that is a signature of increasing lattice defects [33]. It is worth to note that in the case of doping-like defects the increase of position of G mode with impurity degree is instead accompanied by an increasing stiffness [33].

This general behavior is confirmed by the Raman spectra in the wavenumber range of 2500–2800 cm^{-1} , reported in Fig. 5b. In this range, graphite is characterized by a broad peak (designed as 2D mode) centered at about 2685 cm^{-1} . Differently from the G mode, the position of this peak depends on the laser excitation wavelength λ (in our case λ = 632.8 nm) [33–35]. The differences with respect to graphite become gradually more significant when spectra of the sample obtained from KNO_3 to that one derived from $NaClO_3$ are considered, in the order indicated in Fig. 5b. Beyond the pristine graphite 2D mode (at 2685 cm^{-1}), the fit of the experimental data requires an additional component at about 2648 cm^{-1} with increasing intensity. This mode becomes the prevalent one in the samples obtained by using $NaIO_4$ and $NaClO_3$ as oxidizers. Two dotted lines represent the position of these two modes in Fig. 5b. The observed shift of the 2D mode position to lower wavenumber values with respect to pristine graphite is a signature of presence of graphene sheets, indicating the formation of low stage GICs [19]. A large intercalation configuration in the $NaIO_4$ and $NaClO_3$ systems is inferred because the Raman signal results generated by almost monolayers of graphene (low stage number). In the remaining samples, intercalation process is also obtained but with relative thicker layer blocks of graphite (high stage number) interposed to intercalated layers. The thermogravimetric behavior of different GICs was evaluated by thermogravimetric analysis (TGA) (Fig. 6). TGA runs from 25 to 800 °C at heating rate of 10 °C min^{-1}. During the thermal treatment, an expansion phenomenon of GICs occur [13]. Intercalating agent and graphite react according to the following scheme [36, 37].

$$C + 2H_2SO_4 \rightarrow CO_2 + 2SO_2 + 2H_2O \quad (2)$$

According to this scheme, there is a release of gases during the GIC's expansion: carbon dioxide, sulfur dioxide, and water vapor. The weight loss, due to the gas released, can be clearly seen for all the considered samples. The weight loss ranged from 3%, for KNO_3, up to 52% for $NaClO_3$ (Table 3). The order of data in Table 3, in increasing degree of weight loss, is the same as that used to tabulate μ-RS results in Fig. 5, and it clearly indicates that highest intercalation degree corresponds to higher weight loss.

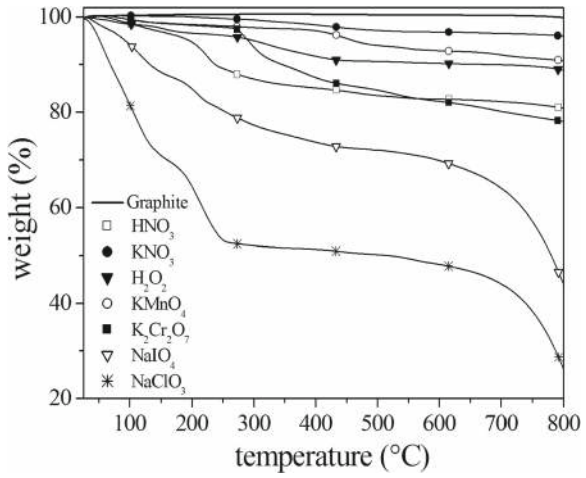

Fig. 6 TGA results for graphite and graphite intercalated compounds

Conclusions

We have presented and described new chemical routes for synthetizing highly intercalated graphite bisulfate. The reaction schemes use different auxiliary reagents (oxidizing agent): nitric acid, potassium nitrate, potassium dichromate, potassium permanganate, sodium periodate, sodium chlorate, and hydrogen peroxide. Micro-Raman spectroscopy analysis of products has shown that samples treated by $NaIO_4$ and $NaClO_3$ lead to final products with the highest intercalation degree, which is consistent with the weight loss from the TGA data. Furthermore, according to FT-IR data, OH is the only oxygen-containing group generated during the intercalation process. EDS elemental analysis allowed to assess the presence of sulfur and oxygen characterizing the oxidation/intercalation process. The SEM micrographs, FT-IR analysis, micro-Raman spectroscopy, and calculated weight loss (from TGA analysis) confirm that the GIC, obtained using KNO_3 as oxidizer, is the most similar to natural graphite, whereas GIC based on $NaClO_3$ seems to have a higher degree of intercalation.

Table 3 Weight loss percentage of pure graphite flakes and GICs

Sample	Weight loss (%)
Natural graphite	0
KNO_3	3
$KMnO_4$	7
H_2O_2	10
HNO_3	17
$K_2Cr_2O_7$	18
$NaIO_4$	30
$NaClO_3$	52

Abbreviations
EDS: Energy-dispersive X-ray spectroscopy; FT-IR: Fourier transform infrared (spectroscopy); GIC: Graphite intercalated compound; SEM: Scansion electron microscope; TGA: Thermogravimetric analysis; XRD: X-ray powder diffraction; μ-RS: micro-Raman spectroscopy

Acknowledgements
The authors gratefully acknowledge M. C. Del Barone of laboratory "LaMEST" of CNR-IPCB for SEM analysis and M. R. Marcedula and M. De Angioletti of the Laboratory of "Thermal analysis" of CNR-IPCB for FT-IR and thermogravimetric analysis.

Authors' contributions
MS with GC and VA conceived the experimental design and contributed to fabrication of samples. MS wrote part of the paper. GC, SDN and C. Cam participated to the characterization of samples and helped to draft the manuscript. C. Car. participated in the design of the experiment and coordination. All authors have read and approved the final manuscript.

Authors' information
MS is a materials engineer. She received her degree from the University of Naples Federico II, Italy, in 2013. During her thesis, she worked at CNR-ICTP Institute and her research was focused on bio-polymer-based nanocomposites. At present, she is a Ph.D. student in "Industrial Product and Process Engineering" at the University of Naples Federico II (Dept. DICMaPI). She works at the CNR-IPCB Institute, and her scientific interest is focused on carbon chemistry, nanostructures, and 2D materials. G.C. (Dr) is a senior researcher of the CNR at the Institute CNR-IPCB. His present research interests are in the field of advanced functional materials based on polymer-embedded inorganic nanostructures. In particular, his activity concerns the development of new chemical routes for the controlled synthesis of metal and semiconductor clusters in polymeric matrices, the fabrication of devices based on properties of nanoscopic objects (e.g., luminescence of quantum dots and tunable surface plasmon absorption of nano-sized noble metal alloys), and the investigation of mechanisms involved in atomic and molecular cluster formation in polymeric media (nucleation, growth, aggregation, etc.) by optical and luminescence spectroscopy. He has authored 180 research articles published in international journals, 10 patents, and many conference papers. He is the editor of two Wiley books devoted to metal-polymer nanocomposites, and he is a member of the editorial board of different scientific journals. S. De N. received his BS degree in physics from the University of Naples Federico II, Italy, in 1982. From 1983 to 1987, he was a system analyst at Elettronica (Rome) and Alenia (Naples). He has been staff researcher at the Institute of Cybernetics "E. Caianiello" of the CNR and at National Institute of Optics (CNR-INO). Currently, he is senior researcher at the CNR-SPIN Institute. He has been a scientific coordinator of the research project "Imaging techniques for studying and analyzing microstructured materials" of the Dept. of Phys. Sci. and Matter Technologies of CNR. He has been a coordinator of the research unit in the framework of the CNR-FIRB program, Photonic microdevices in lithium niobate. He has contributed to about 300 technical papers in peer-reviewed international journals, book chapters, conference papers, and several patents. His research interests include the development of quantum methodologies to the description of coherent phenomena in many body systems, quantum tomography, theoretical modeling for studying dynamical effects in mesoscopic systems, transport properties in nanostructured polymeric materials and biological media, and optical and electron beam propagation in nonlinear media and plasma. C. Cam. is staff member of CNR since 1984 and at present, is senior researcher at the CNR-SPIN Institute. His research focus is on exploring the electronic and structural properties of superconductor thin films, and electronically strongly correlated materials as iron pnictides and graphene. His research activity includes micro-Raman spectroscopy analysis and development of methods and processes for micro- and nano-structural engineering. V. A. graduated in chemistry in 1997 and got her Ph.D. in materials engineering in 2000 at the University of Naples Federico II, Italy. She is currently an associate professor at the Dept. of Chem., Mat. and Production Engineering of the University of Naples. She is author/co-author of 60 papers in international journals, three book chapters, and one national patent. Her research interests comprise the synthesis, modification, and characterization of thermoplastic and thermosetting polymers, CNT/polymer composites, and stimuli-responsive/active polymer-based systems. C. Car. is a full professor of Chemistry at the University of Naples Federico II. Since 2001, he is director of the Institute of Polymers, Composites and Biomaterials of CNR (CNR-IPCB). He is coordinator of the sponsored project of CNR, Special Materials for Advanced Technologies, and responsible for the research project BRITE-EURAM. He is an author of 170 international papers and 10 patents. Currently, his research interests are focused on polymer chemistry and technology, polymer functionalization, polymer synthesis, liquid crystalline polymers, composites and nanocomposites, functional and smart textiles, recycling and processing of plastics, advanced materials for packaging, use of natural products as additive of polymers, and nutraceuticals for polymers.

Competing interests
The authors declare that they have no competing interests.

Author details
[1]CNR-IPCB, Institute for Polymers, Composites and Biomaterials, P.le E. Fermi, 1, 80055 Portici, Italy. [2]Department of Chemical, Materials and Production Engineering, University of Naples Federico II, P.le Tecchio, 80, 80125 Naples, Italy. [3]CNR-SPIN, Institute for Superconductors, Innovative Materials and Devices, S.S. Napoli, Complesso Universitario di M.S. Angelo, Via Cinthia, 80126 Naples, Italy.

Received: 23 November 2016 Accepted: 18 February 2017
Published online: 06 March 2017

References
1. Dresselhaus MS, Dresselhaus G (1994) New directions in intercalation research. Molecular Crystals, Liquid Crystals, Science and Technology Sect. A - Molecular Crystals and Liquid Crystals 244:1–12
2. Chung DDL (2002) Review: graphite. J Mater Sci 37:1475–1489
3. Zhao W, Tan PH, Liu J, Ferrari AC (2001) Intercalation of few-layer graphite flakes with $FeCl_3$: Raman determination of Fermi level, layer by layer decoupling, and stability. J Am Chem Soc 133:5941–5946
4. Zhang H, Wu Y, Sirisaksoontorn W, Remcho VT, Lerner MM (2016) Preparation, characterization, and structure trends for graphite intercalation compounds containing pyrrolidinium cations. Chem Mater 28:969–974
5. Tian S, Qi L, Wang H (2016) Difluoro(oxalate)borate anion intercalation into graphite electrode from ethylene carbonate. Solid State Ionics 291:42–46
6. Dimiev AM, Ceriotti G, Behabtu N, Zakhidov D, Pasquali M, Saito R, et al. (2013) Direct real-time monitoring of stage transition in graphite intercalation compounds. ACSNano 7:2773–2780
7. Enoki T, Suzuki M, Endo M (2003) Graphite intercalation compounds and applications. University Press, London
8. Caswell N, Solin SA (1978) Vibrational excitations of pure $FeCl_3$ and graphite intercalated with ferric chloride. Solid State Commun 27:961–967
9. Underhill C, Leung SY, Dresselhaus G, Dresselhaus MS (1979) Infrared and Raman spectroscopy of graphite-ferric chloride. Solid State Commun 29:769–774
10. Cheng HS, Sha XW, Chen L, Cooper AC, Foo ML, Lau GC, et al. (2009) An enhanced hydrogen adsorption enthalpy for fluoride intercalated graphite compounds. J Am Chem Soc 131:17732–17733
11. Gruneis A, Attaccalite C, Rubio A, Vyalikh DV, Molodtsov SL, Fink J, et al. (2009) Electronic structure and electron-phonon coupling of doped graphene layers in KC8. Phys Rev B 79:205106
12. Gruneis A, Attaccalite C, Rubio A, Vyalikh DV, Molodtsov SL, Fink J, et al. (2009) Angle-resolved photoemission study of the graphite intercalation compound KC8: a key to graphene. Phys Rev B 80:075431
13. Chung DDL (1987) Review: exfoliation of graphite. J of Materials Sci 22:4190–4198
14. Matsumoto R, Hoshina Y, Azukawa N (2009) Thermoelectric properties and electrical transport of graphite intercalation compounds. Mater Trans 50:1607–1611
15. Takada Y (2016) Theory of superconductivity in graphite intercalation compounds. arXiv:1601–02753
16. Setton R (1987) Intercalation compounds of graphite and their reactions in preparative chemistry using support reagent. Academic Press, San Diego
17. Wang L, Zhu Y, Guo C, Zhu X, Liang L, Qian Y (2014) Ferric chloride-graphite intercalation compounds as anode materials for **L**i-ion batteries. Chem Sus Chem 7:87–91

18. Carotenuto G, De Nicola S, Palomba M, Pullini D, Horsewell A, Hansen T. W. e. a. (2012) Mechanical properties of low-density polyethylene filled by graphite nanoplatelets. Nanotechnology 23:485705
19. Carotenuto G, Longo A, De Nicola S, Camerlingo C, Nicolais L (2013) A simple mechanical technique to obtain carbon nanoscrolls from graphite nanoplatelets. Nanoscale Res Lett 8:403
20. Melezhyk A, Galunin E, Memetov N (2015) Obtaining graphene nanoplatelets from various graphite intercalation compounds. IOP Conf Series: Mat Sci Eng 98:012041
21. Carotenuto G, Longo A, Nicolais L, De Nicola S, Pugliese E, Ciofini M, et al. (2015) Laser- induced thermal expansion of H_2SO_4-intercaleted graphite lattice. J Phys Chem C 119:15942–15947
22. Boehm HP, Setton R, Stumpp E (1994) Nomenclature and terminology of graphite intercalation compounds. Pure and Appl Chem 66:1893–1901
23. Yakovlev AV, Finaenov AI, Zabud'kov SL, Yakovleva EV (2006) Thermally expanded graphite: synthesis, properties and prospects for use. Russian J App Chemistry 79:1741–1751
24. Herold A (1979) Crystallo-chemistry of carbon intercalation compounds. In: Levy F (ed). Intercalated Layered Materials. Springer, Dordrecht. pp 323–421
25. Matsumoto R, Okabe T (2015) Electrical conductivity and air stability of $FeCl_3$, $CuCl_2$, $MoCl_5$ and $SbCl_5$ graphite intercalation compounds prepared from flexible graphite sheets. Synth Met 212:62–68
26. Fauchard M, Cahen S, Lagrange P, Marech JF, Hérold C (2013) Gold nano-sheets intercalated between graphene planes. Carbon 65:236–242
27. Assouik J, Hajji L, Boukir A, Chaouqi M, Lagrange P (2016) Heavy alkali metal-arsenic alloy-based graphite intercalation compounds: investigation of their physical properties. C R Chimie:1–9. doi:10.1016/j.crci.2016.04.005
28. Inagaki M, Tanaike O (1995) Host effect on the formation of sodium-tetrahydrofuran-graphite intercalation compounds. Synth Met 73:77–81
29. Schafhäutl C (1840) Ueber die verbindungen des kohlenstoffes mit silicium, eisen und anderen metallen, welche die verschiedenen gallungen von roheisen, stahl und schmiedeeisen bilden. J Prakt Chem 21:129–157
30. Brodie B (1855) Note sur un nouveau procédé pour la purification et la désagrégation du graphite. Ann Chem Physique 45:351–352
31. Rudorff W (1939) Kristallstruktur der saeureverbindungen des graphits. Z Phys Chem 42:42–69
32. Benoit JM, Buisson JP, Chauvet O, Godon QC, Lefrant S (2002) Low-frequency Raman studies of multiwalled carbon nanotubes: experiments and theory. Phys Rev B 66:013417
33. Casiraghi C, Pisana S, Ferrari AC, Novoselov KS, Geim AK, Ferrari AC (2007) Raman fingerprint of charged impurities in graphene. App Phys Lett 91:233108
34. Roy D, Angeles-Tactay E, Brown RJC, Spencer SJ, Fry T, Dunton TA, et al. (2008) Synthesis and Raman spectroscopic characterisation of carbon nanoscrolls. Chem Phys Lett 465:254–257
35. Cançado LG, Jorio A, Martins Ferreira EH, Stavale F, Achete CA, Capaz RB, et al. (2011) Quantifying defects in graphene via Raman spectroscopy at different excitation energies. Nano Lett 11:3190–3196
36. Camino G, Duquensne S, Delobel R, Eling B, Lindsay C, Roels T (2001) Mechanism of expandable graphite fire retardant action in polyurethanes. ACS Symposium series 797:90–109
37. Duquesne S, Le Bras M, Bourbigot S, Delobel R, Camino G, Eling B, Lindsay C, Roels T (2001) Thermal degradation of polyurethan/expandable graphite coatings. Polym Degrad Stab 74:493–499